Journal of Materials Chemistry C

Accepted Manuscript

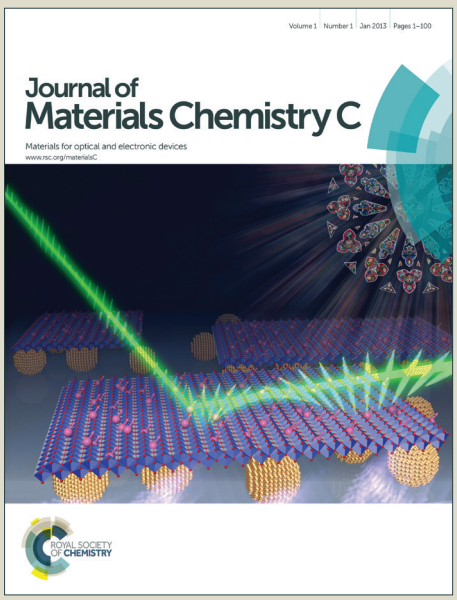

ROYAL SOCIETY OF CHEMISTRY

www.rsc.org/materialsC

Synthesis and Properties of Low Bandgap Star Molecules TPA-[DTS-PyBTTh$_3$]$_3$ and DMM-TPA[DTS-PyBTTh$_3$]$_3$ for Solution Processed Bulk Heterojunction Organic Solar Cells

Kimin Lim[a], Seung Yeon Lee[b,c], Kihyung Song[c], G. D. Sharma[*,d] and Jaejung Ko[*,a]

[a]Department of Materials Chemistry, Korea University 2511 Sejong-Ro, Sejong 339-700, Republic of Korea. Fax: +44-867-5396; Tel: +82-44-860-1337; E-mail: jko@korea.ac.kr
[b]Department of Earth Science, Korea National University of Education, Chungbuk, 363-791, Republic of Korea
[c]Department of Chemical Education, Korea National University of Education, Chungbuk, 363-791, Republic of Korea
[d]R & D center for Engineering and Science, JEC group of colleges, Jaipur Engineering College campus, Kukas, Jaipur (Raj.), India; E-mail: gdsharma273@gmail.com, sharmagd_in@yahoo.com

Two symmetrical planar star shaped organic small molecules **TPA[DTS-PyBTTh$_3$]$_3$ (1)** and **DMM-TPA[DTS-PyBTTh$_3$]$_3$ (2)** with TPA and fused TPA core donors, respectively and three branched DTS-PyBTTh$_3$ units were synthesized and characterized. These small molecules were used donor materials along with $PC_{71}BM$ acceptor for solution processed bulk heterojunction (BHJ) solar cells. The power conversion efficiency (PCE) of the solar cells based on **1** and **2** is about 2.87% and 3.83%, respectively, when the active layers were processed from chlorobenzene (CB) solvent. The higher PCE of the solar cell based on **1** may be attributed to its low bandgap and broad absorption profile as compared to **2**. The PCE of the solution processed BHJ solar cells was improved up to 3.88% and 5.81% for **1** and **2**, respectively, when active layers were processed with 0.4% (v/v) 1-chloronaphthalene (CN) as additive in the CB solvent. The enhancement in the PCE was mainly due to the increase in J_{sc} and *FF*. The increase in the J_{sc} and *FF* may be attributed to the balance charge transport between the electron and hole transport and reduction in the bimolecular recombination, leading to an increase in the PCE.

Key words : Star type small molecules, Fused TPA core, Bulk heterojunction organic solar cells, Power conversion efficiency, Solvent additives.

* corresponding authors

Introduction

Organic solar cells (OSCs) have attracted much attention due to their potential in low cost solar energy harvesting compared with silicon based solar cells, as well as promising applications in flexible, light weight, and large area devices [1-4]. The bulk heterojunction (BHJ) solar cells that contain a blend film of a conjugated material and fullerene derivatives, such as phenyl-C_{61} or C_{71}-butyric acid methyl ester ($PC_{61}BM$ or $PC_{71}BM$) as the active layer has been studied most extensively [5-8]. Through the optimization of molecular structure and device architecture, the power conversion efficiency (PCE) about 10% have been achieved recently [9, 10], giving the hope for the prospects of commercialization. At present, the most efficient donor used for BHJ OSCs are low bandgap semiconducting polymers composed of thieno[3,4-*b*]thiophene and benzodithiophene (poly(thieno[3,4-*b*]thiophene-alt-benzodi-thiophene) (PTB) series. The BHJ OSCs fabricated using these materials and [6,6]-phenyl-C($_{61}$ or $_{71}$)-butyric acid methyl ester (PC ($_{61}$ or $_{71}$)BM) have achieved PCE of up to 9.2% [11]. These OSCs with potential applications in next generation solar cells can compete with inorganic solar cells and dye sensitized solar cells. However, polymer based materials suffer from poor reproducibility of the weight average molecular weight, high dispersity and difficulties in purification.

Meanwhile, OSCs using small molecules as electron donors have also received an increasing attention due to the advantages of easy synthesis and purification, well defined structures, good charge mobility and better batch to batch reproducibility [4, 12-18]. A PCE higher than 8% has recently been reported due to the excellent solubility in organic solvents, broad band light absorption and good charge transport property of the solution processed SM donor [19, 20]. Chen and co-workers have achieved a PCE of 8.12% by developing a series of novel SM donors with a benzodithiophene core, a terthiophene spacer, and a rhodamine end-group [21]. Very recently, Bazan *et al.* reported an OSCs based on the small molecules donor of *p*-DTS(FBTTh$_2$)$_2$ [14, 22, 23] and found that the barium cathode layer can significantly enhance the *FF* of the device via increasing the charge collection at the cathode. Ultimately, the PCE is improved to 9.02% and is the record value for small molecules OSCs, thus making solution processed small molecules OSCs strong competitors to polymer solar cells.

Most of the small molecules as donor materials for photovoltaic applications normally contain four key constituents: donor / acceptor units, conjugated bridges, heteroatom substituents and side chains. The creative design, choice of donor or acceptor units, conjugated bridges and heteroatom substitutions has been successfully overcome the

shortcomings of unbalanced charge transport and poor film quality of small molecules OSCs [24-27]. By tailoring and substituting the functional groups including donor units, acceptor units, and conjugated bridge, star shaped small molecules with low bandgap and strong and broader absorption, together with highly ordered and interconnected domain can be designed resulting in higher PCE of the OSCs [28-32].

Triphenylamine (TPA) is a representative unit to construct star shaped small molecules, due to its good electron donating and high hole transporting abilities. Shang *et al.* have reported a symmetrical star shaped acceptor-donor–acceptor (A-D-A) small molecule compromising of a TPA core and various acceptors [24, 33-36]. Recently, Min *et al*., have developed a star type TPA small molecule N(Ph-2T-DCN-Me) and used as donor component for the fabrication of BHJ solar cells with $PC_{71}BM$ as acceptor and achieved a PCE of 4.76% [30]. Inspired by their work, we have synthesized the star shape small molecules with TPA and fused TPA donor cores for OSCs and achieved a PCE of 4.16% [37]. We have also reported various symmetric and unsymmetric push-pull chromophores for solution processed small molecules OSCs [34-36]. The use of such push-pull type structure in small molecules enables efficient intramolecular charge transfer (ICT), providing better molar extinction coefficient and low bandgap [14]. Moreover, an electron donating group such as TPA can play an important role in stabilizing the separated hole from an exciton and improving the hole transporting properties [37-39].

The electron acceptor unit, thiadiazolo[3,4-*c*]pyridine (PyBT), has also been explored as a strong electron acceptor in the design of low bandgap copolymers [40, 41] with high PCE. Recently, Bazan *et al*. have also explored the PyBT based small molecules and copolymers for solution processed OSCs [46-48].

Recently, we have designed two symmetrical star shaped A-D-A small molecules with fluorine substituted benzothiadiazole electron deficient unit and achieved a PCE of 5.16% for organic solar cells processed with chlorobenzene (CB) and DIO/CB solvent, respectively [49]. These small molecules showed the optical absorption profile up to 700 nm. To increase the optical absorption profile further, we have used PyBT electron acceptor instead of fluorine substituted benzothiadiazole and designed two symmetrical star shape small molecules (Figure 1) **TPA-[DTS-PyBTTh$_3$]$_3$ (1)** and **DMM-TPA[DTS-PyBTTh$_3$]$_3$ (2)**. The incorporation of PyBT leads to extend the optical absorption profile towards NIR region, leading an increased light harvesting efficiency. We have utilized these small molecules as the electron donor along with $PC_{71}BM$ as the electron acceptor for the BHJ solar cells and achieved PCE of 2.87% and 3.83% for **1** and **2**, respectively. When solvent additive 1-

chloronaphthalene (CN) was incorporated into the host CB solvent, the PCE has been improved up to 3.88% and 5.81% for **1** and **2**, respectively.

Experimental details

Measurements and instruments

^{1}H NMR and ^{13}C NMR spectra were recorded on a Varian Mercury 300 spectrometer. Elemental analyses were performed with a Carlo Elba Instruments CHNS-O EA 1108 analyzer. Mass Spectra (MALDI-TOF) were measured by the SNU NCIRF on a Voyager-DEMTM STR Biospectrometry Workstation. The absorption and photoluminescence spectra were recorded on a Perkin-Elmer Lambda 2S UV-visible spectrometer and a Perkin LS fluorescence spectrometer, respectively. Cyclic voltammetry was carried out with a BAS 100B (Bioanalytical System, Inc.). A three electrode system consisted of non-aqueous Reference Electrode (0.1 M Ag/Ag^{+} acetonitrile solution; MF-2062, Bioanalytical System, Inc.), platinum working electrode (MF-2013, Bioanalytical System, Inc.), and a platinum wire (diam. 1.0 mm, 99.9% trace metals basis, Sigma-Aldrich) as counter electrode. Redox potential of dyes was measured in CH_2Cl_2 with 0.1 M $(n\text{-}C_4H_9)_4N\text{-}PF_6$ with a scan rate between 50 mV s^{-1}(vs. Fc/Fc^{+}).

Synthesis of TPA-[DTS-PyBTTh$_3$]$_3$ and **DMM-TPA[DTS-PyBTTh$_3$]$_3$**

7-Bromo-4-(3,3'-dihexylsilylene-2,2'-bithiophen-5-yl)-[1,2,5]thiadiazolo[3,4-*c*]pyridine (7) : 4,7-Dibromo-[1,2,5]thiadiazolo[3,4-*c*]pyridine (0.60 g, 2.03 mmol), (3,3'-dihexylsilylene-2,2'-bithiophen-5-yl)trimethylstannane (**3**) (1.06 g, 2.03 mmol), $Pd(PPh_3)_4$ (0.12 g, 0.1 mmol), and anhydrous toluene (60 ml) were added to a flame-dried 2-neck round-bottom flask with a condenser under a nitrogen atmosphere. The reaction mixture was heated to reflux for 15 hr. The reaction mixture was then cooled to room temperature. The organic layer was separated and dried over anhydrous magnesium sulfate. The solvent was removed in *vacuo*. The product was purified by column chromatography. (eleuent: Mc/Hx = 1/6). Yield: 76%. ^{1}H NMR (300 MHz, $CDCl_3$): δ 8.66 (s, 1H), 8.61 (s, 1H), 7.37 (d, 1H, J = 4.2 Hz), 7.13 (d, 1H, J = 4.8 Hz), 1.42-1.23 (m, 16H), 1.00-0.81 (m, 10H). ^{13}C NMR (75 MHz, $CDCl_3$): δ 156.4, 155.2, 149.1, 148.4, 147.7, 146.3, 145.9, 145.3, 141.1, 136.2, 130.2, 127.1, 107.2, 33.1, 31.7, 24.4, 22.8, 14.3, 12.1. Anal. Calcd. for $C_{25}H_{30}BrN_3S_3Si$: C, 52.07; H, 5.24. Found: C, 52.11; H, 5.21.

4-(3,3'-Dihexylsilylene-2,2'-bithiophen-5-yl)-7-(5''-hexyl-2,2',2''-terthiophen-5-yl)-[1,2,5]thiadiazolo[3,4-*c*]pyridine (8) : 7-Bromo-4-(3,3'-dihexylsilylene-2,2'-bithiophen-5-yl)-[1,2,5]thiadiazolo[3,4-*c*]pyridine (**7**) (0.81 g, 1.40 mmol), (5''-hexyl-2,2',2''-terthiophen-5-

yl)trimethylstannane (**4**) (0.83 g, 1.69 mmol), $Pd(PPh_3)_4$ (0.08 g, 0.07 mmol), and anhydrous toluene (50 ml) were added to a flame-dried 2-neck round-bottom flask with a condenser under a nitrogen atmosphere. The reaction mixture was heated to reflux for 15 hr. The reaction mixture was then cooled to room temperature. The organic layer was separated and dried over anhydrous magnesium sulfate. The solvent was removed in *vacuo*. The product was purified by column chromatography. (eleuent: Mc/Hx = 1/3) Yield: 80%. ^{1}H NMR (300 MHz, $CDCl_3$): δ 8.79 (s, 1H), 8.67 (s, 1H), 8.03 (d, 1H, J = 3.3 Hz), 7.35 (d, 1H, J = 4.2 Hz), 7.25 (d, 1H, J = 3.3 Hz), 7.20 (d, 1H, J = 3.3 Hz), 7.13 (d, 1H, J = 4.2 Hz), 7.05 (d, 1H, J = 4.2 Hz), 7.02 (d, 1H, J = 3.3 Hz), 6.71 (d, 1H, J = 3.3 Hz), 2.83 (t, 2H, J = 7.5 Hz), 1.71 (m, 2H), 1.41-1.24 (m, 22H), 1.03-0.82 (m, 13H). ^{13}C NMR (75 MHz, $CDCl_3$): δ 155.1, 154.8, 149.2, 148.7, 146.6, 146.1, 145.8, 144.5, 144.4, 143.1, 140.9, 138.9, 135.9, 135.6, 135.1, 130.1, 128.4, 127.5, 125.1, 124.9, 124.5, 124.3, 123.8, 123.7, 119.4, 36.6, 36.3, 36.2, 32.2, 30.8, 29.5, 23.6, 23.2, 18.3, 18.1, 14.6, 11.5. Anal. Calcd. for $C_{43}H_{49}N_3S_6Si$: C, 62.35; H, 5.96. Found: C, 62.38; H, 5.94.

4-(5'-Bromo-3,3'-dihexylsilylene-2,2'-bithiophen5-yl)-7-(5''-hexyl-2,2',2''-terthiophen-5-yl)-[1,2,5]thiadiazolo[3,4-c]pyridine (9) : 4-(3,3'-Dihexylsilylene-2,2'-bithiophen-5-yl)-7-(5''-hexyl-2,2',2''-terthiophen-5-yl)-[1,2,5]thiadiazolo[3,4-*c*]pyridine (**8**) (0.91 g, 1.10 mmol) was dissolved in 100 mL of $CHCl_3$. Then NBS (0.20 g, 1.15 mmol) was added by portions and the mixture was stirred for 12 h at RT under dark condition. The organic layer was separated and dried over anhydrous magnesium sulfate. The solvent was removed in *vacuo*. The product was purified by column chromatography. (eleuent: Mc/Hx = 1/3) Yield: 98%. ^{1}H NMR (300 MHz, $CDCl_3$): δ 8.77 (s, 1H), 8.64 (s, 1H), 8.02 (d, 1H, J = 3.9 Hz), 7.25 (d, 1H, J = 3.9 Hz), 7.19 (d, 1H, J = 3.9 Hz), 7.08 (s, 1H), 7.04 (d, 1H, J = 3.9 Hz), 7.01 (d, 1H, J = 3.0 Hz), 6.70 (d, 1H, J = 3.9 Hz), 2.83 (t, 2H, J = 7.5 Hz), 1.71 (m, 2H), 1.42-1.25 (m, 22H), 1.00-0.83 (m, 13H). ^{13}C NMR (75 MHz, $CDCl_3$): δ 155.1, 154.7, 149.3, 148.7, 146.5, 146.0, 145.9, 144.5, 144.3, 143.1, 140.9, 138.9, 135.9, 135.6, 135.1, 130.1, 128.4, 127.5, 125.1, 124.9, 124.5, 123.8, 123.7, 119.4, 111.8, 36.6, 36.3, 36.2, 32.1, 30.7, 29.4, 23.6, 23.1, 18.4, 18.1, 14.5, 11.5. Anal. Calcd. for $C_{43}H_{48}BrN_3S_6Si$: C, 56.93; H, 5.33. Found C, 56.91; H, 5.30.

Tris((4-(3,3'-dihexylsilylene-2,2'-bithiophen-5-yl)-7-(5''-hexyl-2,2',2''-terthiophen-5-yl)-[1,2,5]thiadiazolo[3,4-*c*]pyridine)-*p*-phenylene)amine (TPA-[DTS-PyBTTh$_3$]$_3$):

In a Ar filled glove box a 50 mL microwave tube was charged with tris(4-(trimetylstannyl)phenyl)amine (**5**) (100 mg, 0.136 mmol), 4-(5'-bromo-3,3'-dihexylsilylene-2,2'-bithiophen5-yl)-7-(5''-hexyl-2,2',2''-terthiophen-5-yl)-[1,2,5]thiadiazolo[3,4-*c*]pyridine (**9**) (445 mg, 0.491 mmol), $Pd(PPh_3)_4$ (8 mg, 0.007 mmol), toluene (40 mL), and sealed with

a Teflon® cap. The reaction mixture was heated to 120 °C for 5 minutes, 140 °C for 5 minutes, and 175 °C for 90 minutes, using a Biotage microwave reactor. After cooling, the organic layer was separated and dried over anhydrous magnesium sulfate. The solvent was removed in *vacuo*. The purple product was purified by column chromatography. (eleuent: Mc/Hx = 1/1 and 2% triethylamine) Yield: 63%. ^{1}H NMR (300 MHz, $CDCl_3$): δ 8.75 (s, 3H), 8.65 (s, 3H), 8.00 (d, 3H, J = 3.9 Hz), 7.53 (d, 3H, J = 7.8 Hz), 7.23 (d, 3H, J = 3.9 Hz), 7.18-7.10 (m, 12H), 7.03 (d, 3H, J = 3.6 Hz), 7.00 (d, 3H, J = 3.0 Hz), 6.70 (d, 3H, J = 3.0 Hz), 2.82 (t, 6H, J = 7.5 Hz), 1.71 (m, 6H), 1.47-1.21 (m, 66H), 1.04-0.83 (m, 39H). Anal. Calcd. for $C_{147}H_{156}N_{10}S_{18}Si_3$: C, 64.81; H, 5.77. Found: C, 64.83; H, 5.75. MS (MALDI-TOF): Calcd. for $C_{156}H_{168}N_{10}S_{18}Si_3$, 2724.31; found, 2724.46.

Tris((4-(3,3'-dihexylsilylene-2,2'-bithiophen-5-yl)-7-(5''-hexyl-2,2',2''-terthiophen-5-yl)-[1,2,5]thiadiazolo[3,4-c]pyridine)-2,6,10-yl)-4,4,8,8,12,12-hexamethyl-*4H*,*8H*,*12H*-benzo[1,9]quinolizino[3,4,5,6,7,-*defg*]acridine (DMM-TPA[DTS-PyBTTh$_3$]$_3$) :

In a Ar filled glove box a 50 mL microwave tube was charged with 2,6,10-trimethylstannyl-4,4,8,8,12,12-hexamethyl-*4H*,*8H*,*12H*-benzo[1,9]quinolizino[3,4,5,6,7,-defg]acridine (**6**) (100 mg, 0.117 mmol), 4-(5'-bromo-3,3'-dihexylsilylene-2,2'-bithiophen5-yl)-7-(5''-hexyl-2,2',2''-terthiophen-5-yl)-[1,2,5]thiadiazolo[3,4-*c*]pyridine (**9**) (383 mg, 0.422 mmol), $Pd(PPh_3)_4$ (7 mg, 0.006 mmol), toluene (40 mL), and sealed with a Teflon® cap. The reaction mixture was heated to 120 °C for 5 minutes, 140 °C for 5 minutes, and 175 °C for 90 minutes, using a Biotage microwave reactor. After cooling, the organic layer was separated and dried over anhydrous magnesium sulfate. The solvent was removed in *vacuo*. The purple product was purified by column chromatography. (eleuent: Mc/Hx = 1/1 and 2% triethylamine) Yield: 59%. ^{1}H NMR (300 MHz, $CDCl_3$): δ 8.79 (s, 3H), 8.70 (s, 3H), 8.02 (d, 3H, J = 3.0 Hz), 7.67-7.65 (m, 9H), 7.24 (s, 3H), 7.19 (d, 3H, J = 3.3 Hz), 7.04 (d, 3H, J = 3.9 Hz), 7.01 (d, 3H, J = 3.0 Hz), 6.69 (d, 3H, J = 3.0 Hz), 2.82 (t, 6H, J = 7.5 Hz), 1.71 (m, 6H), 1.62 (s, 18H), 1.52-1.28 (m, 66H), 1.10-0.88 (m, 39H). Anal. Calcd. for $C_{156}H_{168}N_{10}S_{18}Si_3$: C, 65.87; H, 5.95. Found: C, 65.89; H, 5.94. MS (MALDI-TOF): Calcd. for $C_{156}H_{168}N_{10}S_{18}Si_3$, 2844.50; found, 2844.61.

Fabrication of photovoltaic devices and characterization

The BHJ films were prepared as follow: The indium tin oxide (ITO)-coated glass substrate was first cleaned with detergent, ultrasonicated in acetone and isopropyl alcohol, and subsequently dried overnight in an oven. PEDOT:PSS (Heraeus, Clevios P VP.AI 4083) in aqueous solution was spin-cast to form a film with thickness of approximately 50 nm. The substrate was dried for 10 min at 140 °C in air and then transferred into a glove box to spin-

cast the photoactive layer. Small molecules were combined with $PC_{71}BM$ blend in several ratios (1:1−1:3 w/w) in CB at a concentration of 30 mg mL^{-1}. The blend solutions were spin-cast on the PEDOT layer, and the substrate was dried for 2 h. Then, a thin film of Al (90 nm thick) was deposited on top of the active layer.

All the devices were fabricated and tested in ambient atmosphere without encapsulation. The active area of the devices is about 0.20 cm^2. The hole and electron only devices ITO/PEODT:PSS/**donor**:$PC_{71}BM$/Au and Al/**donor**:$PC_{71}BM$/Al structures, were fabricated to measure the hole and electron mobility, respectively.

The current–voltage characteristics of the devices were measured using a computer controlled Keithley 238 source meter under AM1.5 illumination (100 mW cm^{-2}). A xenon light source coupled with AM1.5 optical filter was used as light source to illuminate the surface of the devices. The incident photon to current efficiency (IPCE) of the devices was measured by illuminating the device through the light source and monochromator and resulting current was measured using Keithley electrometer under short circuit condition

Results and discussion

Synthesis of TPA-[DTS-PyBTTh$_3$]$_3$ (1) and DMM-TPA[DTS-PyBTTh$_3$]$_3$ (2)

Scheme 1 illustrates the synthetic protocol of organic small molecules **TPA-[DTS-PyBTTh$_3$]$_3$** (**1**) and **DMM-TPA[DTS-PyBTTh$_3$]$_3$** (**2**) starting from the 4-(3,3'-dihexylsilylene-2,2'-bithiophen-5-yl)-7-(5''-hexyl-2,2',2''-terthiophen-5-yl)-[1,2,5]thiadiazolo[3,4-*c*]pyridine (**8**), which was synthesized from the Stille coupling reaction of 4,7-dibromo-[1,2,5]thiadiazolo[3,4-*c*]pyridine, (3,3'-dihexylsilylene-2,2'-bithiophen-5-yl)trimethylstannane (**3**), followed by the Stille coupling reaction with (5''-hexyl-2,2',2''-terthiophen-5-yl)trimethylstannane (**4**). The 4-(5'-bromo-3,3'-dihexylsilylene-2,2'-bithiophen5-yl)-7-(5''-hexyl-2,2',2''-terthiophen-5-yl)-[1,2,5]thiadiazolo[3,4-*c*]pyridine (**9**) was synthesized by bromination of **8** with NBS in $CHCl_3$. The compounds **1** and **2** were synthesized via a microwave assisted Stille coupling reaction between the brominated molecular 'wing' **9** and the stannylated molecular 'core' of either tris(4-(trimetylstannyl)phenyl)amine (**3**) or 2,6,10-trimethylstannyl-4,4,8,8,12,12-hexamethyl-*4H*,*8H*,*12H*-benzo[1,9]quinolizino[3,4,5,6,7,-defg]acridine (**4**).

Optical and electrochemical properties

Figure 2 shows the UV–visible absorption spectra of **1** and **2**, respectively, in CB and thin film form. The corresponding optical properties are complied in Table 1. As shown in Figure 2, the absorption spectra of **1** and **2** exhibited two typical absorption bands in 300–800 nm. The absorption bands observed at lower energies (longer wavelengths) were originated

from the ICT between the highest occupied molecular orbital (HOMO) and lowest unoccupied molecular orbital (LUMO). The absorption bands at 300–430 nm were dominated by the HOMO–1 → LUMO excitation that may be assigned to the π–π* transitions. As shown in Figure 2 and Table 1, the ICT bands of **1** and **2** in solution showed molar extinction coefficients of 156,000 M^{-1} cm^{-1} at 620 nm and 137,000 M^{-1} cm^{-1} at 630 nm, respectively. In addition, these two small molecule **1** and **2** have a motif similar to that of highly efficient symmetrical A–D–A organic semiconductor DTS-$(PTTh_2)_2$, which compromises a DTS donor and two [1,2,5]-thiadiazolo[3,4-c]pyridine (PT) acceptor end capped with hexylbithiophene (Th_2). These molecules exhibit broad band absorptions and good hole mobility [14].

As shown in Figure 1, absorption bands in thin film of both **1** and **2** were more broad and red–shifted by 15 nm and 25 nm, respectively, as compared to those in solution. This suggests that the strong intermolecular π-π interaction and aggregation exists in the solid state [50, 51]. The optical bandgap of **1** and **2** were calculated to be 1.67 eV and 1.62 eV by the absorption onset 742 nm and 766 nm, respectively. These values are slightly less than those estimated from absorption and emission cross peak CB solution.

Figure 3 shows UV–visible absorption spectra of **1**:$PC_{71}BM$ (1:2) and **2**:$PC_{71}BM$ (1:2) films. The ICT bands of **1** and **2** observed in **1**:$PC_{71}BM$ and **2**:$PC_{71}BM$ blend films, respectively were similar and slightly blue shifted relative to those in solid state film. These results indicate that the $PC_{71}BM$ may significantly interrupt the intermolecular π–π packing interactions between the p-type organic semiconductors by interacting with PyBT moieties of **1** and **2** in the blend films.

The HOMO and LUMO energy levels of the small molecules were estimated from the oxidation and reduction onsets, respectively, observed in cyclic voltammograms of these materials under the assumption that energy level of ferrocene (Fc) was 4.8 eV below the vacuum level. The calculated HOMO/LUMO levels of **1** and **2** were –4.96/–3.56 eV and –5.05/–3.62 eV, respectively, and the corresponding values are summarized in Table 1. The values of LUMO of both **1** and **2** are sufficiently higher than the LUMO of $PC_{71}BM$ (–4.1 eV), indicating that efficient photoinduced charge separation is possible and can be used as donors for the BHJ OSCs.

Theoretical calculations and molecule simulation

The electronic properties of **1** and **2** have also investigated by theoretical calculations. Figure 4 shows the optimized structures of **1** and **2**, which were calculated by TD–DFT using

the B3LYP functional/6–31G* basis set. The orbital densities of the HOMOs of **1** and **2** were evenly distributed on TPA core. But the orbital densities of LUMOs and LUMO+1 of these materials were located on PyBT moiety. The calculations revealed that the ICT from TPA 'core' (HOMO) to PyBT 'wing' (LUMO and LUMO+1) can effectively occur in **1** and **2** when excited by light energy.

Hole mobility

The hole mobility is an important parameter for effective charge transport and collection in the organic solar cells. The hole mobility of **1** and **2** films was measured by space charge limited current (SCLC) method with the device structure ITO/PEDOT:PSS/**1** or **2**/Au, using the current voltage characteristics in dark. The hole mobilities estimated from SCLC method were about 6.3 x 10^{-5} cm^2 V^{-1} s^{-1} and 7.1 x 10^{-5} cm^2 V^{-1} s^{-1}, for **1** and **2**, respectively. The planar structure of **2** may leads to an enhanced transport via efficient intermolecular π–π packing interactions.

Photovoltaic properties

Small molecules **1** and **2** were employed as donor (D) for fabrication of photovoltaic devices along with $PC_{71}BM$ as acceptor (A) with different weight ratio i.e. 1:1, 1:2 and 1:3. The weight ratio of spin D:A (1:2) for both the small molecules gave the best photovoltaic performance. We have chosen $PC_{71}BM$ instead of $PC_{61}BM$ as acceptor counter part, since the former has a superior spectral response in visible region. Figure 5a displays the current-voltage (*J-V*) characteristics under 1.5 AM irradiation (100 mW cm^{-2}) OSC fabricated from **1** or **2**:$PC_{71}BM$ (1:2 wt ratio) and corresponding values are summarized in Table 2. The higher value of PCE for **1**:$PC_{71}BM$ (2.87%) active layer than **2**:$PC_{71}BM$ (3.83%) has been attributed to the increased values of J_{sc}, V_{oc} and *FF*. The device based on small molecule **1**:$PC_{71}BM$ active layer exhibited higher V_{oc} (0.82 V) as compared to that for **2**:$PC_{71}BM$ (0.74 V), owing to its lower laying HOMO energy level. The relatively higher J_{sc} and *FF* for the device based on **2** could be attributed to the better hole mobility resulting from the efficient intermolecular π–π packing interactions, due to its planar skeleton. The benzene rings in TPA have ~35 degree of tilted angle on a nitrogen atom, while the tilt angle in DMM-TPA was much smaller because of the DMM bridge between the benzene rings [37]. Moreover, the radical cation of DMM TPA had a nearly planar structure. Thus, we supposed that the DMM-TPA core can facilitate intermolecular packing and increase the lifetime of the charge-separated state in the BHJ system more efficiently than does TPA. The IPCE spectra of these devices were shown in Figure 5b and the IPCE spectra of devices were well matched with the optical

spectra of blends, resulting in a close correlation with the photocurrents with *J-V* characteristics.

The PCE of the BHJ solar cells based on either **1** or **2** as donor is relatively low due to the low values of J_{sc} and *FF*. For an efficient organic solar cell, there must be a proper nanomorphology in thin film BHJ active layer for exciton dissociation and balanced charge transport. We assume that the poor PCE using **1** or **2**:$PC_{71}BM$ active layer may be due to an imbalanced charge transport and insufficient nanomorphology of the active layers. Various processing techniques have been developed in order to optimize the nanoscale morphology of the BHJ active layer to improve the PCE of organic solar cells, including thermal annealing [52, 53], solvent annealing [54] and spontaneous inter-diffusion of bi-layer heterojunction [55]. In addition to above processing methods, the use of solvent additives was recently employed to enhance the photovoltaic performance of BHJ OSCs [56-58]. To improve the PCE of organic devices based on **1** and **2**, we have used CN as additive. We have varied the concentration of CN in the solvent from 0.1% to 0.5% by volume and found that the optimized concentration was about 0.4%. Beyond that concentration, the PCE of the solar cell decreases due to the over aggregation of donor phase, which disturbs the percolating pathways of acceptor phase and reducing the electron mobility in the BHJ active layer. The over-aggregation of the donor phase may also reduce the effective interfacial area for charge separation and consequently reduces the photocurrent generation [59, 60]. The reduction in PCE may also be attributed to the incomplete drying of active layer due to the high boiling point of CN. Therefore, we have discussed the effect of solvent additive on the photovoltaic performance of the devices only for the 0.4% (v/v) CN in CB. The *J–V* characteristics of the devices processed with CN/CB under illumination are shown in Figure 6 and the corresponding photovoltaic parameters are compiled in Table 2.

The PCE of the devices for **1** and **2** have been significantly enhanced up to 3.88% and 5.81%, respectively. The increase in the PCE upon addition of CN arises from the enhancement in *FF* and J_{sc}. The increase in J_{sc} and *FF* may be attributed to the favorable nanomorphology for active layer and more balanced charge transport in the device processed from CN/CB solvent.

The morphology of the active layer is also very important for the performance of organic solar cells and strongly depends upon its morphological features. To investigate the enhancement in the PCE for the solar cells based on the active layers processed with CN/CB solvent, we have also used atomic force microscopy (AFM) to get information about the change in the morphology of the active layer with the addition of solvent additive. The AFM

height images for **2**:$PC_{71}BM$ casted with and without CN are shown in Figure 7. Similar AFM images have been observed for **1**:$PC_{71}BM$ thin films. The AFM images showed a different surface morphology and the root mean square (rms) values of **2**:$PC_{71}BM$ are 1.45 nm and 3.56 nm for with and without CN, respectively. Phase separation between small molecule donor and fullerene acceptor in the domain size (10-20 nm) can provide enough D/A interfaces for exciton dissociation. The phase images in both BHJ active layer also indicates that the nano-phase separation is formed. However, with the addition of CN, the spin coated **2**:$PC_{71}BM$ seems more clear than that of the cast using only CB. The lower rms value and clearer nanophase separation therefore lead to higher values of J_{sc} and *FF*, resulting in an enhancement in the overall PCE.

We have also recorded the transmission electron microcopy (TEM) images of active layers processed with and without CN additives (as shown in Figure 8 for **2**:$PC_{71}BM$) to get more information about the phase separation. It can be seen from these images that large size aggregation were clearly observed in the film processed with CB only, however, after the solvent additives the domain sizes are significantly reduced, leading the better phase separation. The better phase separation and reduces domain sizes leads to the more efficient exciton dissociation and charge transport.

Figure 9 shows the X-ray diffraction (XRD) patterns of the **1**: $PC_{71}BM$ and **2**:$PC_{71}BM$ active layers cast on ITO substrates. As shown in the Figure 9a, **1**:$PC_{71}BM$ cast from CB solvent exhibits as a broad and weak peak at $2\theta=4.32°$, indicating low crystallinity. This peak becomes stronger for the film cast from CN/CB solvent, indicating that CN promote the crystallinity of **1** when it is incorporated into CB as additive. It was observed that **2**:$PC_{71}BM$ film (Figure 9b) processed from CB exhibits shows more sharp peak at $2\theta=4.34°$, due to the more crystallinity induced by molecular coplanarity of **2**.

To get the information about the effect of solvent additive on the charge transport in the photovoltaic devices, we have measured the hole and electron mobilities in the blend cast from CB or CN/CB using the hole only (ITO/PEDOT:PSS/blend layer cast from CB or CN/CB/Au and electron only ITO/Al/ blend layer cast from CB or CN/CB/Al devices [28]. The hole and electron mobilities were extracted by fitting the current –voltage characteristics (as shown in Figure) using the Mott-Gurney relationship as described by following expression:

$$J = \frac{9}{8}\varepsilon_o \varepsilon_r \mu \frac{V^2}{d^3}$$

where J is current density, d is the thickness of active blend layer, μ is the charge carrier mobility, ε_o is the permittivity of free space and ε_r is the relative dielectric constant of the transport layer, V is the effective voltage in the device given by $V = V_{appl} - V_{bi}$, where V_{appl} is the voltage applied to the device and V_{bi} is the built in voltage owing to the relative difference in the work functions of two electrodes and have been estimated from the transition between the ohmic and space charge current limited (SCLC) region [61,62]. The hole and electron mobilities for the active layer processed with and without additive were estimated from the plots of $log\ J_d$ versus V (Figure 10). Here we have included the plots only for the devices based on **2**:$PC_{71}BM$ active layers. Similar plots have been observed for the devices based on **1**:$PC_{71}BM$ layers. The values of hole and electron mobilities are summarized in Table 3. The low hole mobility and the unbalanced electron/hole transport lead to the poor PCE of the organic solar cells based on the active layers processed from only CB solvent. The solvent additive enhances the hole mobility significantly. Moreover, the electron mobility is also improved slightly, and more balanced electron/hole transport is obtained. Under the same conditions, both hole and electron mobilities of **1**:$PC_{71}BM$ films are higher than those of **2**:$PC_{71}BM$. Therefore, the more enhanced PCE of **1** is mainly ascribed to its superior charge transport ability due to the planar molecule geometry of fused TPA core and also through the reduction of domain size in active layer.

Conclusions

In summary, we have demonstrated the synthesis, optical, and electrochemical properties of two novel symmetrical planar star molecules **TPA-[DTS-PyBTTh$_3$]$_3$** (**1**) and **DMM-TPA[DTS-PyBTTh$_3$]$_3$** (**2**) and used them as donor component along with $PC_{71}BM$ for the fabrication of solution processed organic BHJ solar cells. The BHJ solar cells based on **1**:$PC_{71}BM$ (1:2) and **2**:$PC_{71}BM$ (1:2) showed overall PCE of 2.87% and 3.83%, respectively. Higher PCE of **2** than **1** as donor has been attributed to an increased values of J_{sc}, FF and V_{oc}. The larger value of J_{sc} and FF has been ascribed to the higher value of hole mobility for **2** as compared to **1** due to the planer core for **2**, which facilitates charge transport more easily. We found that the PCE of the devices is significantly enhanced for the devices when solvent additive (0.4% CN by volume) is used for film processing, resulting in over all PCE of 3.88% and 5.81% for **1** and **2**, respectively. We found that the active layer processed from only CB showed poor phase separation with large domain size, and charge transport is unbalanced, leading to the lower both J_{sc} and FF. However, the device processed with 0.4% (v/v) CN yields a favorable nanoscale morphology, in which phase separation is sufficiently

created a percolating pathway for charge transport. We believe that these finding could bring out new approaches in the development of novel small organic molecules.

Acknowledgements

This research was supported by the International Science and Business Belt Program (2013K000496) and the ERC (the Korean government (MEST)) program (2013004800) through the Ministry of Science, ICT and Future Planning.

References

1. F.C. Krebs, J. Fyenbo and M. Jørgensen, *J. Mater. Chem.,* 2010, **20**, 8994.
2. F.C. Krebs, T. Tromholt and M. Jørgensen, *Nanoscale,* 2010, **2**, 873.
3. G. Li, R. Zhu and Y. Yang, *Nat. Photonics*, 2012, **6**, 153.
4. Y. Lin, Y. Li and X. Zhan, *Chem. Soc. Rev.*, 2012, **41**, 4245.
5. C. M. Amb, S. Chen, K. R. Graham, J. Subbiah, C. E. Small, F. So and J. R. Reynolds, *J. Am. Chem. Soc.*, 2011, **133**, 10062.
6. S. C. Price, A. C. Stuart, L. Yang, H. Zhou and W. You, *J. Am. Chem. Soc.,* 2011, **133**, 4625.
7. T.-Y. Chu, J. Lu, S. Beaupré, Y. Zhang, J.-R. M. Pouliot, S. Wakim, J. Zhou, M. Leclerc, Z. Li, J. Ding and Y. Tao, *J. Am. Chem. Soc.,* 2011, **133**, 4250.
8. Y. Huang, X. Guo, F. Liu, L. Huo, Y. Chen, T. P. Russell, C. C. Han, Y. Li and J. Hou, *Adv. Mater.,* 2012, **23**, 4636.
9. J. You, L. Dou, K. Yoshimura, T. Kato, K. Ohya, T. Moriarty, K. Emery, C. C. Chen, J. Gao, G. Li and Y. Yang, *Nat. Commun.,* 2013, **4**, 1446.
10. L. Dou, J. You, J. Yang, C.-C. Chen, Y. He, S. Murase, T. Moriarty, K. Emery, G. Li and Y. Yang, *Nat. Photonics*, 2012, **6**, 180.
11. Z. He, C. Zhong, S. Su, M. Xu, H. Wu and Y. Cao, *Nat. Photonics* 2012, **6**, 593.
12. W. Cambarau, A. Viterisi, J. W. Ryan and E. Palomares, *Chem. Commun.,* 2014, **50**, 5349.
13. T. S. van der Poll, J. A. Love, T.-Q. Nguyen and G. C. Bazan, *Adv. Mater.*, 2012, **24**, 3646.
14. Y. Sun, G. C. Welch, W. L. Leong, C. J. Takacs, G. C. Bazan and A. J. Heeger, *Nat. Mater.*, 2012, **11**, 44.
15. Y. Yang, J. Zhang, Y. Zhou, G. Zhao, C. He, Y. Li, M. Andersson, O. Inganas and F. Zhang, *J. Phys. Chem. C*, 2010, **114**, 3701.
16. A. Mishra and P. Bäuerle, *Angew. Chem. Int. Ed.*, 2012, **51**, 2020.
17. Y. Chen, X. Wan and G. Long, *Acc. Chem. Res.*, 2013, **46**, 2645.

18. B. Walker, C. Kim and T. Q. Nguyen, *Chem. Mater.*, 2011, **23**, 470.
19. A. K. K. Kyaw, D. H. Wang, D. Wynands, J. Zhang, T.-Q. Nguyen, G. C. Bazan and A. J. Heeger, *Nano Lett.*, 2013, **13**, 3796.
20. A. K. K. Kyaw, D. H. Wang, V. Gupta, W. L. Leong, L. Ke, G. C. Bazan and A. J. Heeger, *ACS Nano*, 2013, **7**, 4569.
21. J. Zhou, Y. Zuo, X. Wan, G. Long, Q. Zhang, W. Ni, Y. Liu, Z. Li, G. He, C. Li, B. Kan, M. Li and Y. Chen, *J. Am. Chem. Soc.*, 2013, **135**, 8484.
22. V. Gupta, A. K. Kyaw, D. H. Wang, S. Chand, G. C. Bazan and A. J. Heeger, *Sci. Rep.*, 2013, **3**, 1965.
23. T. van der Poll, J. Love, T. Nguyen and G. C. Bazan, *Adv. Mater.*, 2013, **25**, 6014.
24. H. X. Shang, H. J. Fan, Y. Liu, W. P. Hu, Y. F. Li and X. W. Zhan, *Adv. Mater.* 2011, **23**, 1554.
25. S. Haid, A. Mishra, M. Weil, C. Uhrich, M. Pfeiffer and P. Bäuerle, *Adv. Funct. Mater.,* 2012, **22**, 4322.
26. J. Y. Zhou, X. J. Wan, Y. S. Liu, Y. Zuo, Z. Li, G. R. He, G. K. Long, W. Ni, C. X. Li, X. C. Su and Y. S. Chen, *J. Am. Chem. Soc.,* 2012, **134**, 16345.
27. Z. Li, G. R. He, X. J. Wan, Y. S. Liu, J. Y. Zhou, G. K. Long, Y. Zou, M. T. Zhang, Y. S. Chen, *Adv. Energy Mater.* 2012, **2**, 74.
28. S. Roquet, A. Cravino, P. Leriche, O. Aleveque, P. Free and J. Roncali, *J. Am. Chem. Soc.* 2006, **128**, 3459.
29. E. Ripaud, T. Rousseau, P. Leriche and J. Roncali, *Adv. Energy Mater.* 2011, **1**, 540.
30. D. Deng, S. L. Shen, J. Zhang, C. He, Z. J. Zhang and Y. F. Li, *Org. Electron.* 2012, **13**, 2546.
31. J. Zhang, Y. Yang, C. He, Y. J. He, G. J. Zhao and Y. F. Li, *Macromolecules* 2009, **42**, 7619.
32. J. Min ,Y. N. Luponosov, A. Gerl, M. S. Polinskaya, S. M. Peregudova, P. V. Dmitryakov, A. V. Bakirov, M. A. Shcherbina, S. N. Chvalun, S. Grigorian, N. Kaush-Busies, S. A. Ponomarenko, T. Ameri and C. J. Brabec, *Adv. Energy mater.* 2014, 4, 1301234.
33. Y. Lin, Y. Wang, J. Wang, J. Hou, Y. Li, D. Zhu and X. Zhan, *Adv. Mater.* DOI: 10.1002/adma.201400525.
34. Y. Lin, Z.-G. Zhang, H. Bai, Y. Li and X. Zhan, *Chem. Commun.*, 2012, **48**, 9655.
35. Y. Lin, P. Cheng, Y. Li and X. Zhan, *Chem. Commun.*, 2012, **48**, 4773.

36. Y. Lin, H. Wang, Y. Li, D. Zhu and X. Zhan, *J. Mater. Chem. A*, 2013, **1**, 14627.
37. S. Park, N. Cho, S. Cho, J.K. Lee and J. Ko, *Org. Lett.,* 2012, **14**, 6329.
38. S. So, H. Choi, H. M. Ko, C. Kim, S. Paek, N. Cho, K. Song, J. K. Lee and J. Ko, *Sol. Energy Mater. Sol. Cells,* 2012, **98**, 224.
39. H. Choi, S. Paek, J. Song, C. Kim, N. Cho and J. Ko, *Chem. Commun.,* 2011, **47**, 5509.
40. J. K. Lee, B. S. Jeong, J. Kim, C. Kim and J. Ko, *J. Photochem. Photobiol. A: Chemistry,* 2013, **251**, 25.
41. S. A. Ponomarenko, S. Kirchmeyer, A. Elschner, B. Huisman, A. Karbach and D. Drechsler, *Adv. Funct. Mater.*, 2003, **13**, 591.
42. J. Lee, M. H. Yun, J. Kim, J. Y. Kim and C. Yang, *Macromol. Rapid Commun*. 2012, **33**, 140.
43. J. Lee, J. Kim, G. Kim and C. Yang, *Tetrahedron* 2010, **66**, 9440.
44. N. Blouin, A. Michaud, D. Gendron, S. Wakim, E. Blair, R. Neagu-Plesu, M. Belletete, G. Durocher, Y. Tao and M. Leclerc, *J. Am. Chem. Soc.* 2008, **130**, 732.
45. H. X. Zhou, L .Q. Yang, S. C. Price, K. J. Knight, W. You, *Angew. Chem. Int. Ed.,* 2010, **49**, 7992.
46. G. C. Welch and G. C. Bazan, *J. Am. Chem. Soc.,* 2011, **133**, 4632.
47. Z. B. Henson, G. C. Welch, T. V. Poll and G. C. Bazan, *J. Am. Chem. Soc.,* 2012, **134**, 3766.
48. G. C. Welch, R. C. Bakus, S. J. Teat and G. C. Bazan, *J. Am. Chem. Soc.* 2013, **135**, 2298.
49. N. Cho, S. Paek, J. Jeon, K. Song, G. D. Sharma, J. Ko, *J. Mater. Chem A.,* 2014, **2**, 12368.
50. R. C. Coffin, J. Peet, J. Rogers and G. C. Bazan, *Nat. Chem.,* 2009, **1**, 657.
51. A. Lelige, P. Blanchard, T. Rousseau and J. Roncali, *Org. Lett.* 2011, **13**, 3098.
52. W. Ma, C. Yang, X. Gong, K. Lee and A. J. Heeger, *Adv. Funct. Mater.,* 2005, **15**, 1617.
53. X. Yang, J. Loos, S. C. Veenstra, W. J. H. Verhees, M. M. Wienk, J. M. Kroon, M. A. J. Michels and R. A. J. Janssen, *Nano Lett.,* 2005, **5**, 579.
54. G. Li, V. Shrotriya, J. Huang, Y. Yao, T. Moriarty, K. Emery and Y. Yang, *Nat. Mater.,* 2005, **4**, 864.
55. J. S. Moon, C. J. Takacs, Y. Sun and A. J. Heeger, *Nano Lett.* 2011, **11**, 1036.
56. Y. Yao, J. Hou, Z. Xu, G. Li and Y. Yang, *Adv. Funct. Mater.,* 2008, **18**, 1783.

57. J. S. Moon, C. J. Takacs, S. Cho, R. C. Coffin, H. Kim, G. C. Bazan and A. J. Heeger, *Nano Lett.* 2010, **10**, 4005.
58. J. Peet, J. Y. Kim, N. E. Coates, W. L. Ma, D. Moses, A. J. Heeger and G. C. Bazan, *Nat. Mater.,* 2007, **6**, 497.
59. J. A. Love, C. M. Proctor, J. Liu, C. J. Takacs, A. Sharenko, T. S. van der Poll, A. J. Heeger, G. C. Bazan and T. Q. Nguyen, *Adv. Funct. Mater.,* 2013, **23**, 5019
60. C. J. Takacs, Y. Sun, G. C. Welch, L. A. Perez, X. Liu, W. Wen, G. C. Bazan and A. J. Heeger, *J. Am. Chem. Soc.,* 2012, **134**, 16597.
61. G. Malliaras, J. Salem, P. Brock and C. Scott, *Phys. Rev. B: Condens. Matter Mater. Phys.,* 1998, **58**, 13411.
62. H. Martens, H. Brom and P. Blom, *Phys. Rev. B: Condens. Matter Mater. Phys.,* 1999, **60**, 8489

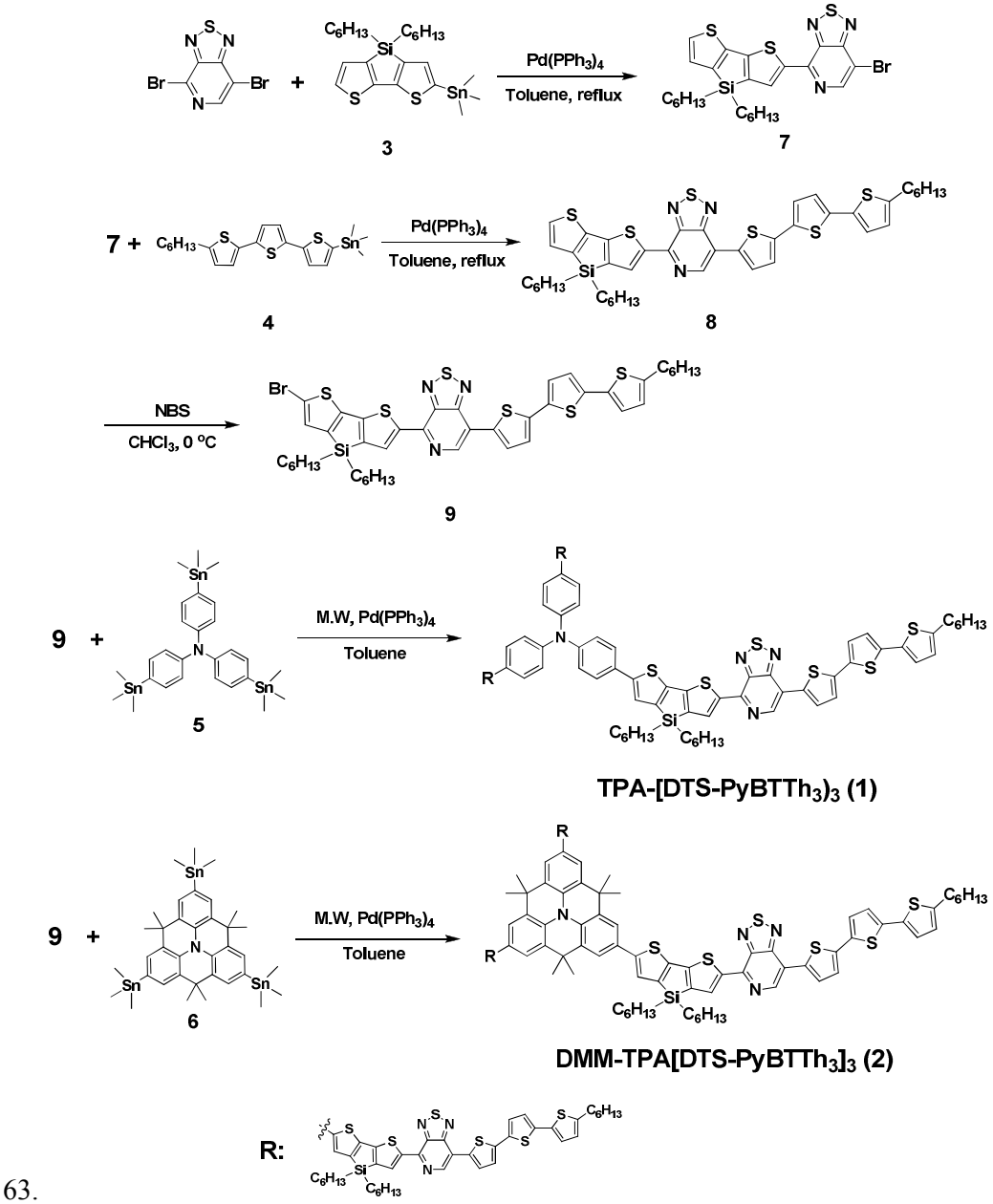

63.

Scheme 1. Schematic diagrams for the synthesis of **1** and **2** small molecules

Table 1. Optical, redox parameters of the compounds

	λ_{abs}[a] (nm) (ε/$M^{-1}cm^{-1}$)	$\lambda_{abs,\ flim}$ (nm)	λ_{PL}[a] (nm)	$E_{onset,\ ox}$(V) / HOMO (eV)[b]	$E_{onset,red}$ (V) / LUMO (eV)[b]	E_{opt} (eV)[c]	E_{0-0} (eV)[d]
1	410 (125,000), 620 (156,000)	635	770	0.16 / -4.96	-1.24 / -3.56	1.75	1.67
2	415 (107,000), 630 (137,000)	655	785	0.25 / -5.05	-1.18 / -3.62	1.73	1.62

[a] Absorption and emission spectra were measured in CB solution. [b] Redox potential of the compounds were measured in dichloromethane with 0.1 M $(n\text{-}C_4H_9)_4NPF_6$ with a scan rate of 50 mV s^{-1} (*vs*. Fc/Fc+). [c] E_{opt} was calculated from the absorption and emission cross peak in CB solution. [d] $E_{0\text{-}0}$ was calculated from the absorption thresholds from absorption spectra in CB solution.

Table 2. Photovoltaic parameters of organic solar cells based on different blends

Small molecules	J_{sc} (mA cm^{-2})	V_{oc} (V)	*FF*	PCE (%)
1:$PC_{71}BM$[a]	8.82	0.74	0.44	2.87
2:$PC_{71}BM$[a]	9.74	0.82	0.48	3.83
1:$PC_{71}BM$[b]	10.66	0.70	0.52	3.88
2:$PC_{71}BM$[b]	12.84	0.78	0.58	5.81

[a]cast from CB, [b]cast from 0.4% (v/v) CN/CB

Table 3. Summary of hole and electron mobilities of **1**:$PC_{71}BM$ and **2**:$PC_{71}BM$ films processed from CB and 0.4% (v/v) CN/CB solvents

Active layer	Solvent	Hole mobility ($cm^2\ V^{-1}\ s^{-1}$)	Electron mobility ($cm^2\ V^{-1}\ s^{-1}$)	Electron/hole mobility ratio
1:$PC_{71}BM$	CB	4.05×10^{-6}	4.65×10^{-4}	115
1:$PC_{71}BM$	CN/CB	3.16×10^{-5}	4.72×10^{-4}	15
2:$PC_{71}BM$	CB	5.38×10^{-6}	5.45×10^{-4}	94
2:$PC_{71}BM$	CN/CB	6.64×10^{-5}	5.48×10^{-4}	8.25

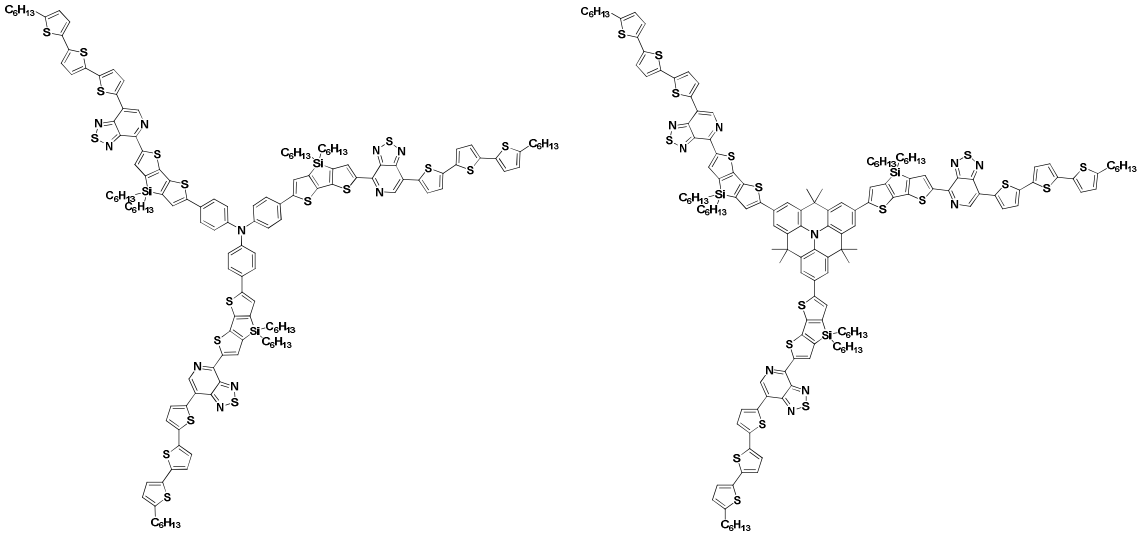

Figure 1. Molecular structures of **TPA-[DTS-PyBTTh$_3$]$_3$** (**1**)and **DMM-TPA[DTS-PyBTTh$_3$]$_3$ (2)**

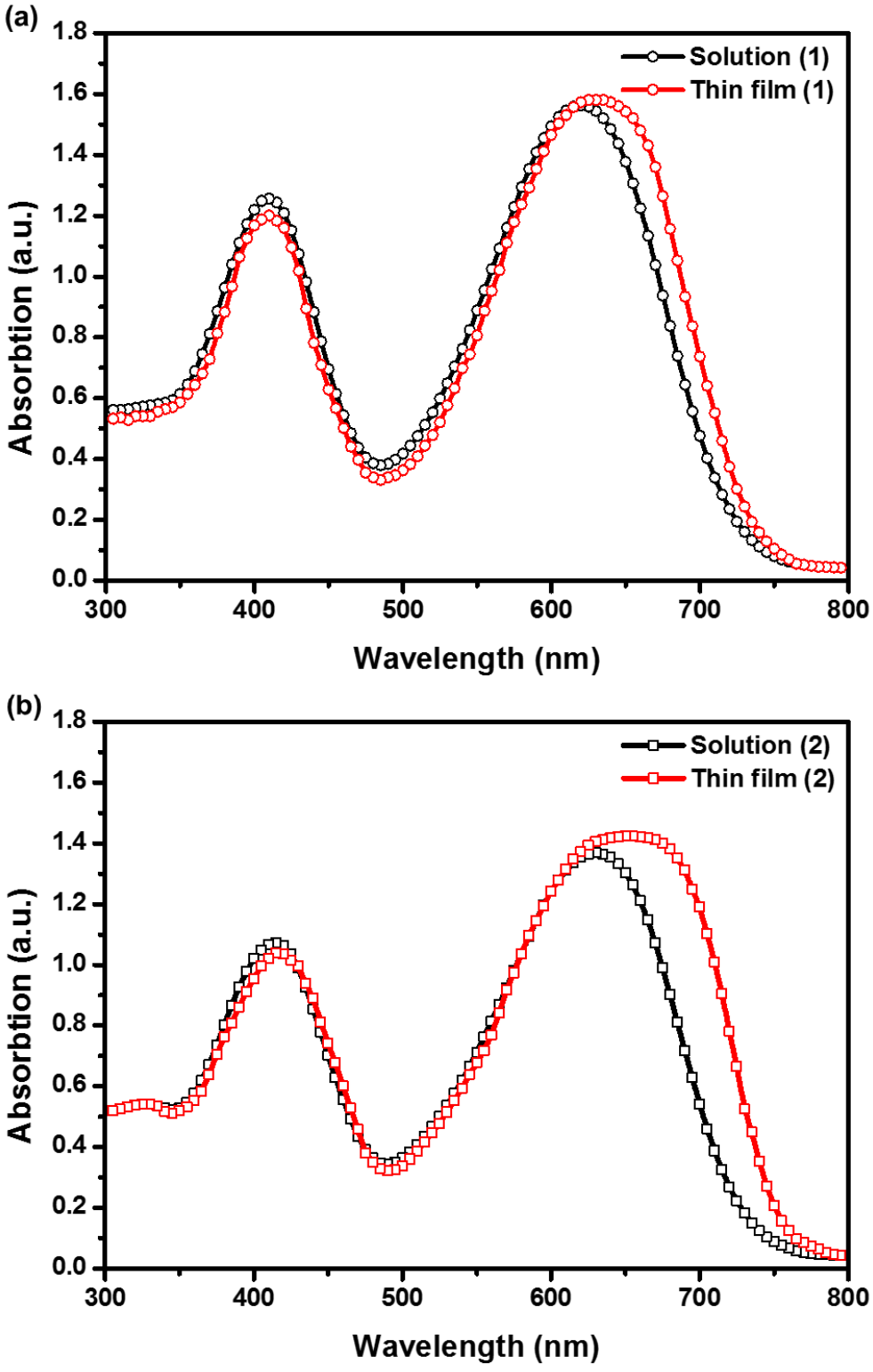

Figure 2. UV-visible absorption spectra of (a) **1** and (b) **2** in CB solution and in thin film form.

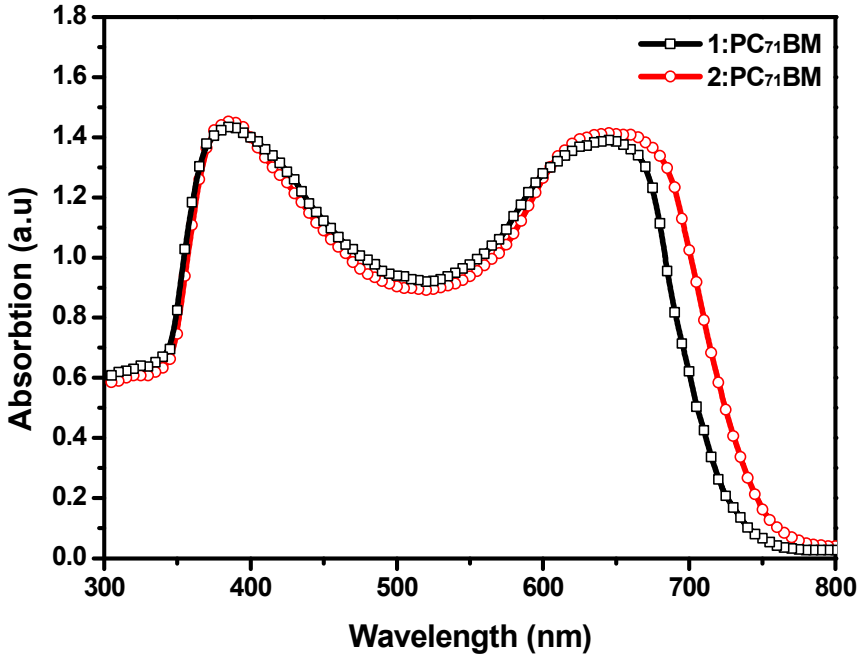

Figure 3. UV-visible spectra of **1**:$PC_{71}BM$ and **2**:$PC_{71}BM$ blend thin films cast from CB

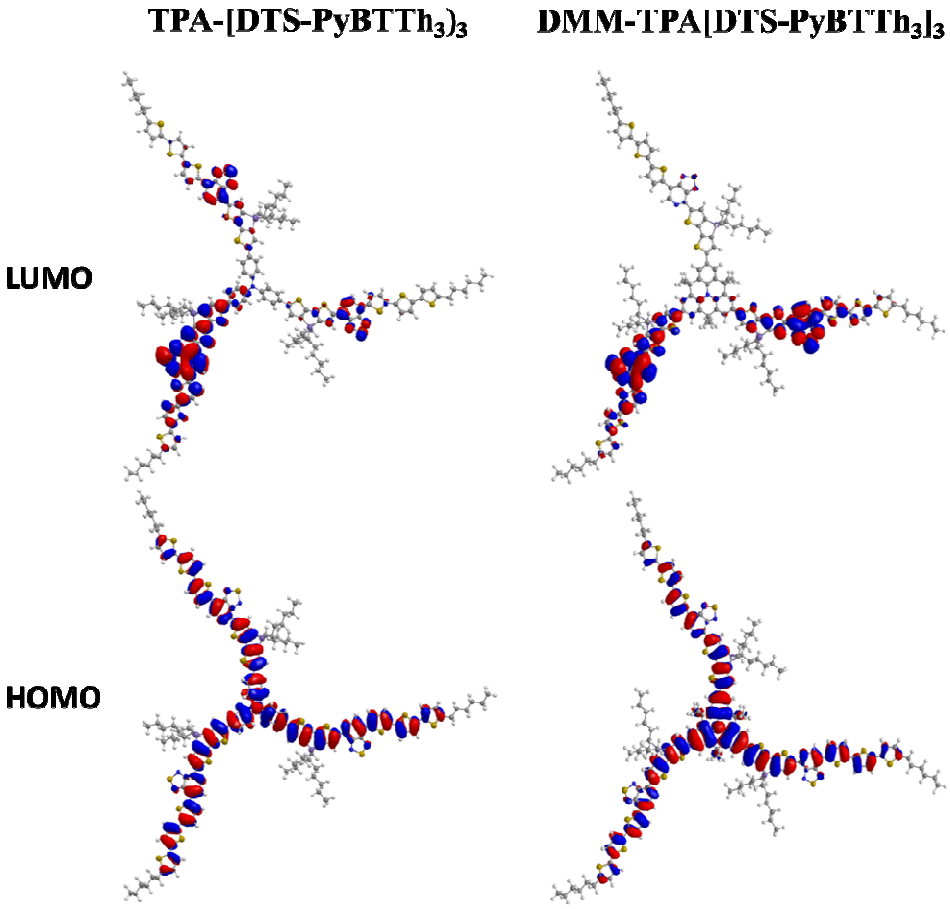

Figure 4. Isodensity surface plots of **1** and **2** calculated by the time dependent-density functional theory (TD-DFT) using the B3LYP functional/6-31G* basis set.

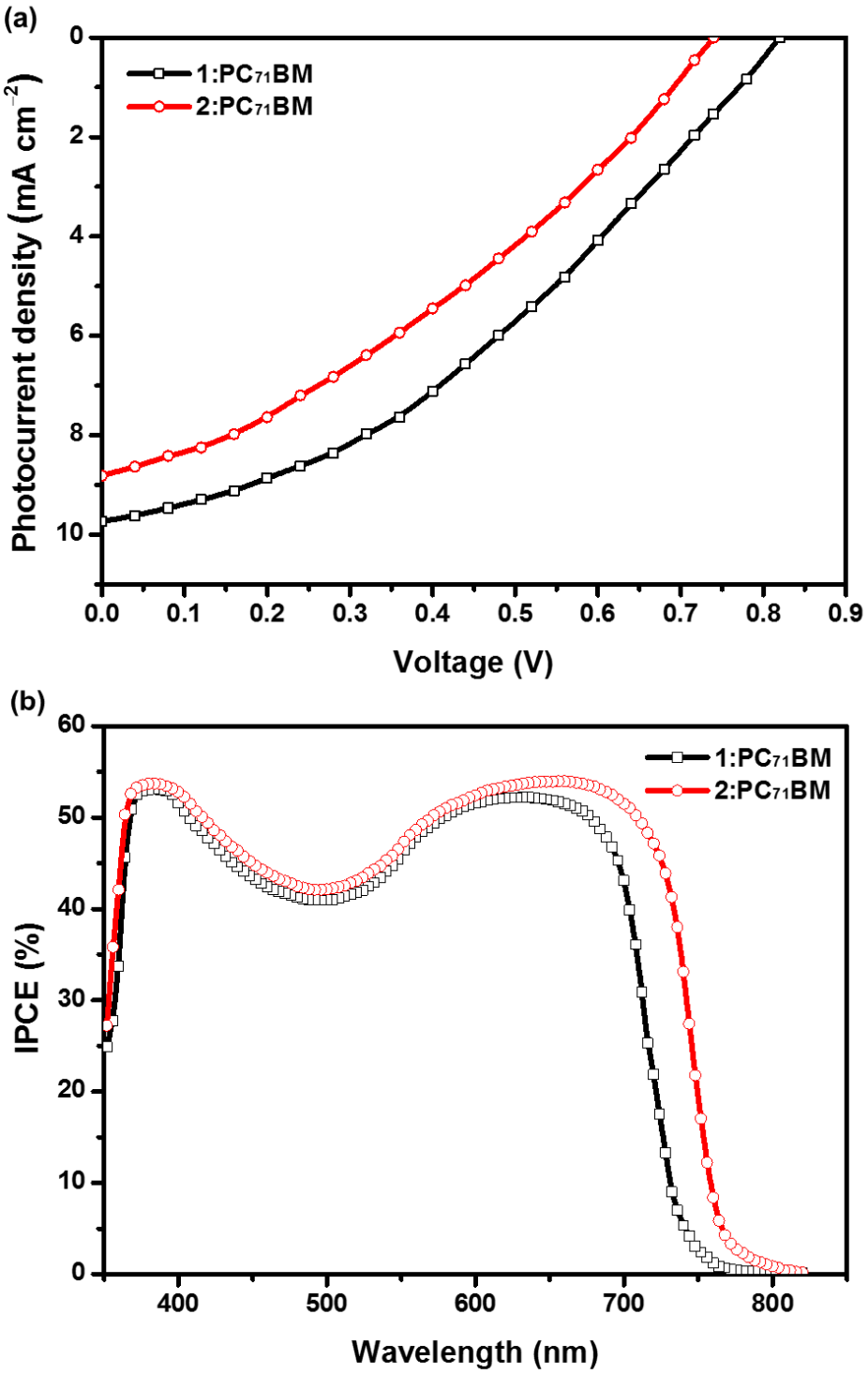

Figure 5. (a) Current –voltage (*J-V*) characteristics under illumination, and (b) IPCE spectra of BHJ solar cells based on **1**:$PC_{71}BM$ and **2**:$PC_{71}BM$ active layers cast from CB.

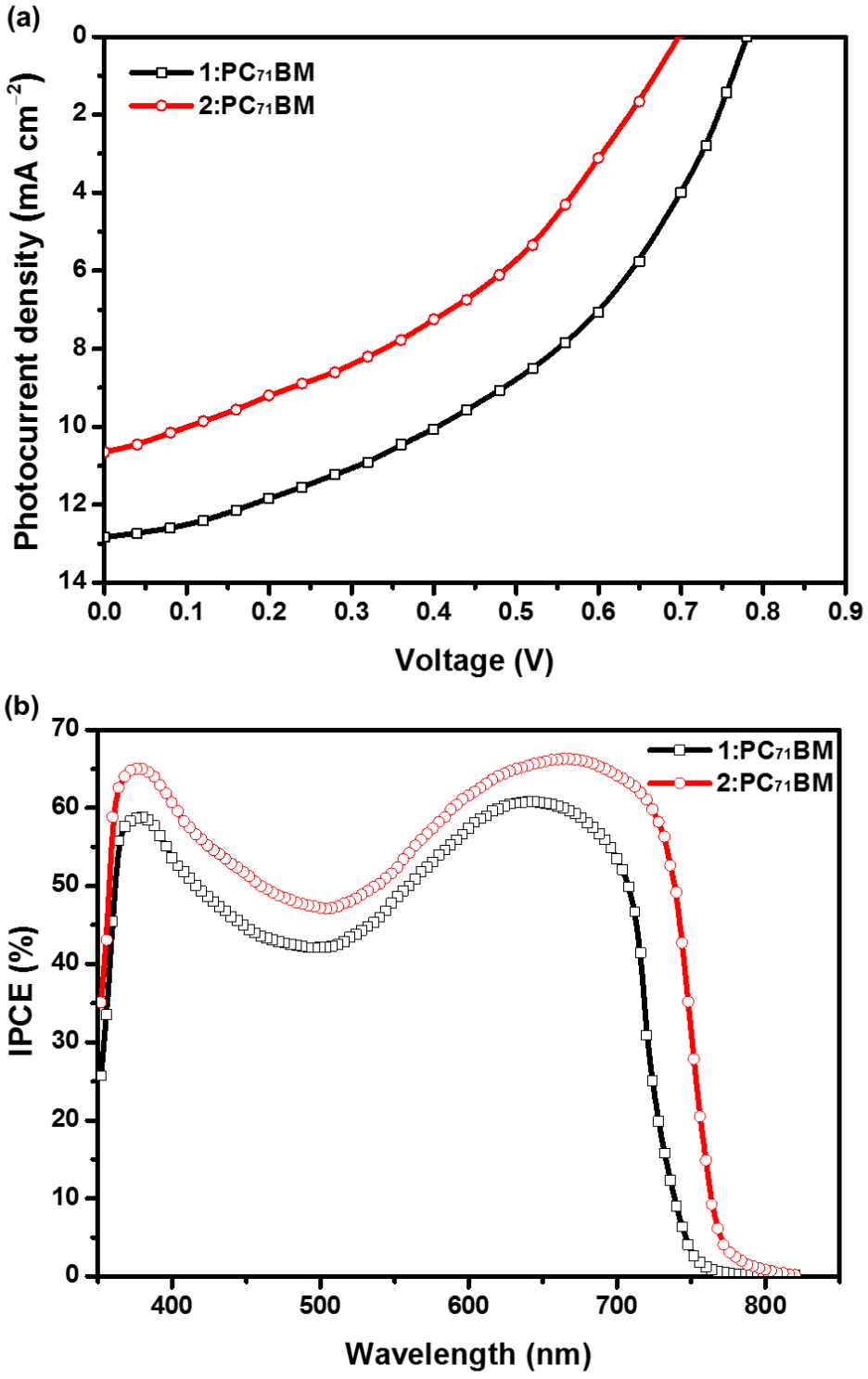

Figure 6. (a) Current –voltage (*J-V*) characteristics under illumination, and (b) IPCE spectra of BHJ solar cells based on **1**:$PC_{71}BM$ and **2:**$PC_{71}BM$ active layers cast from 0.4% (v/v) CN/CB

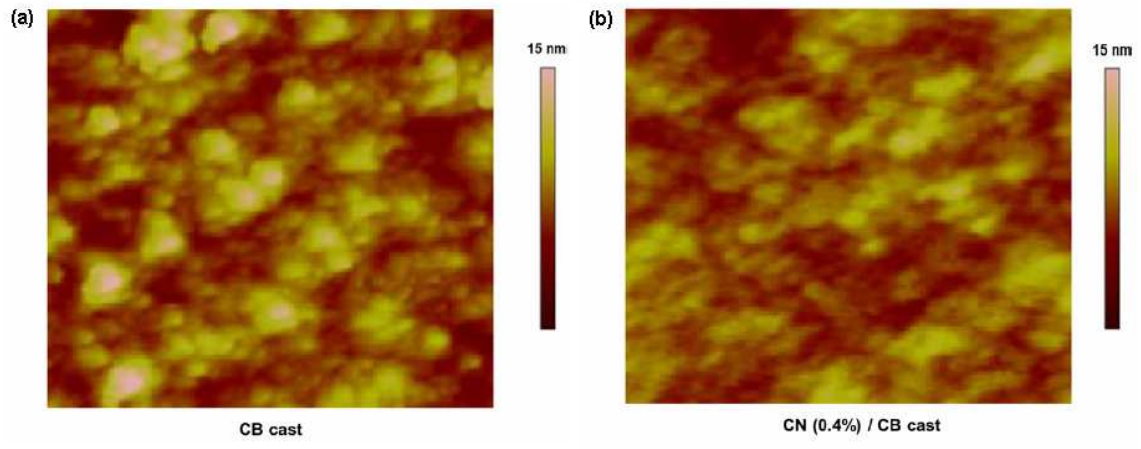

Figure 7. AFM (3 μm x 3 μm) height images for **2**:PC71BM active layer cast from (a) CB and (b) 0.4% (v/v) CN/CB solvents

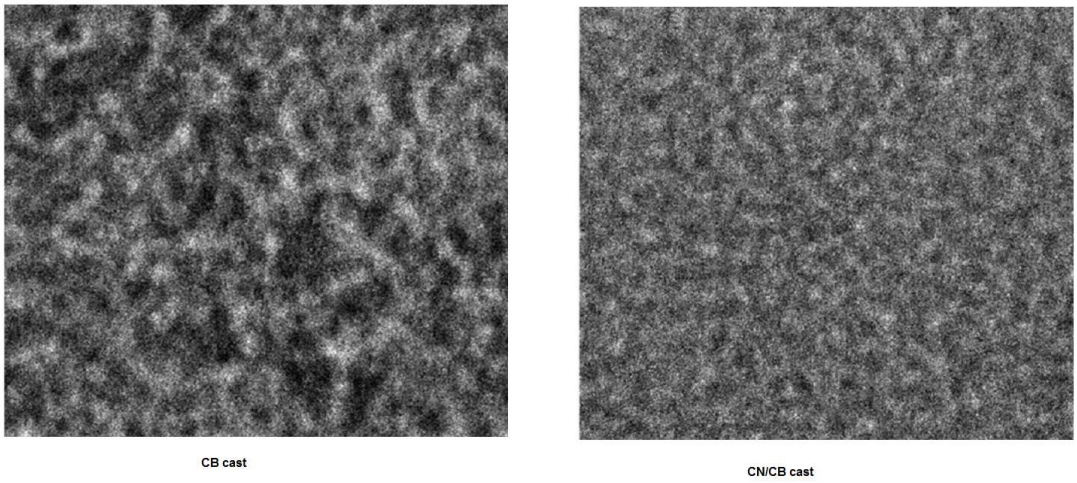

Figure 8. TEM images of the 2:PC71BM blend films processed from CB and CN/CB cast films

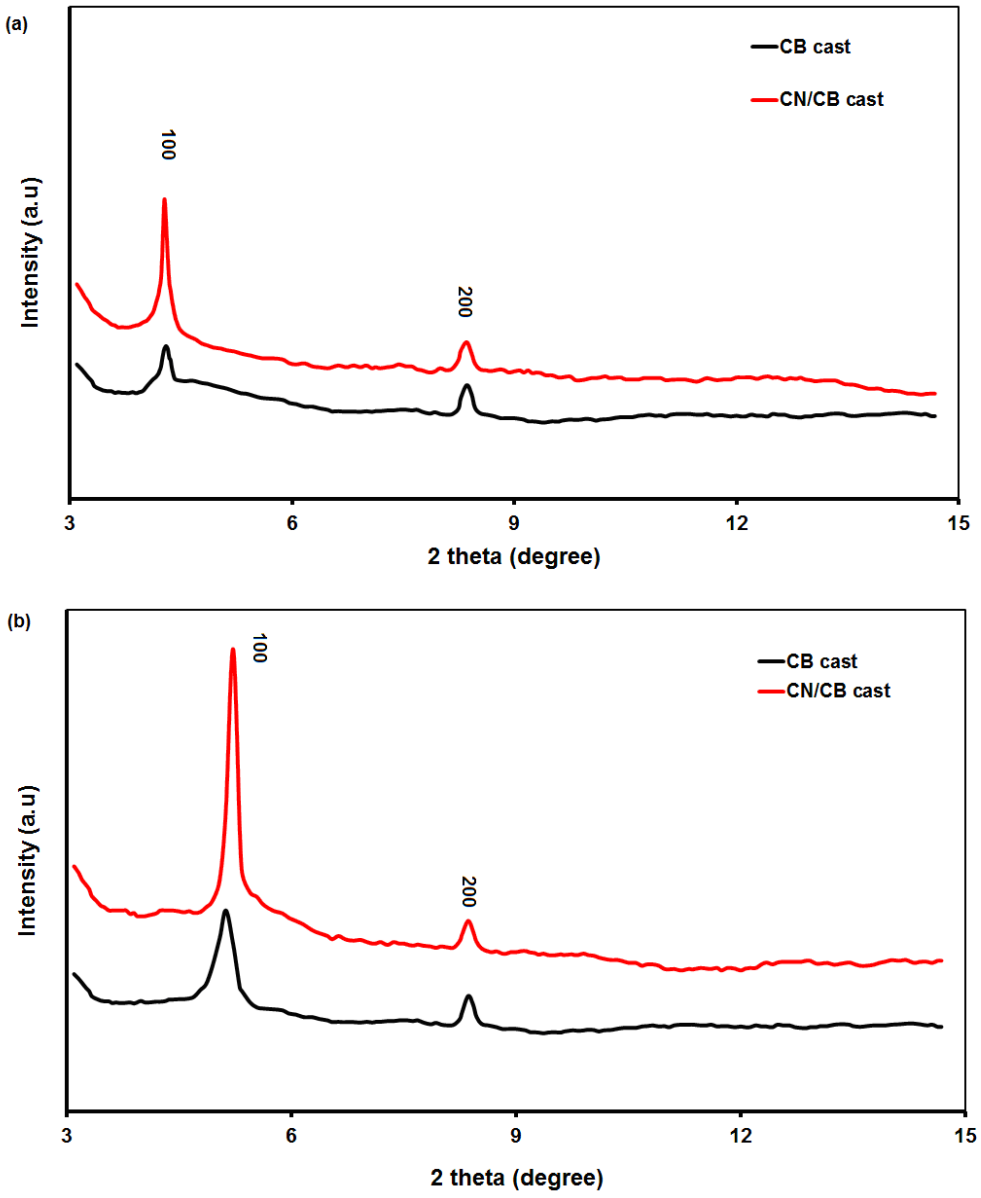

Figure 9. XRD patterns of (a) **1:**$PC_{71}BM$ (b) **2**:$PC_{71}BM$ blend thin films processed from CB and CN/CB solvents

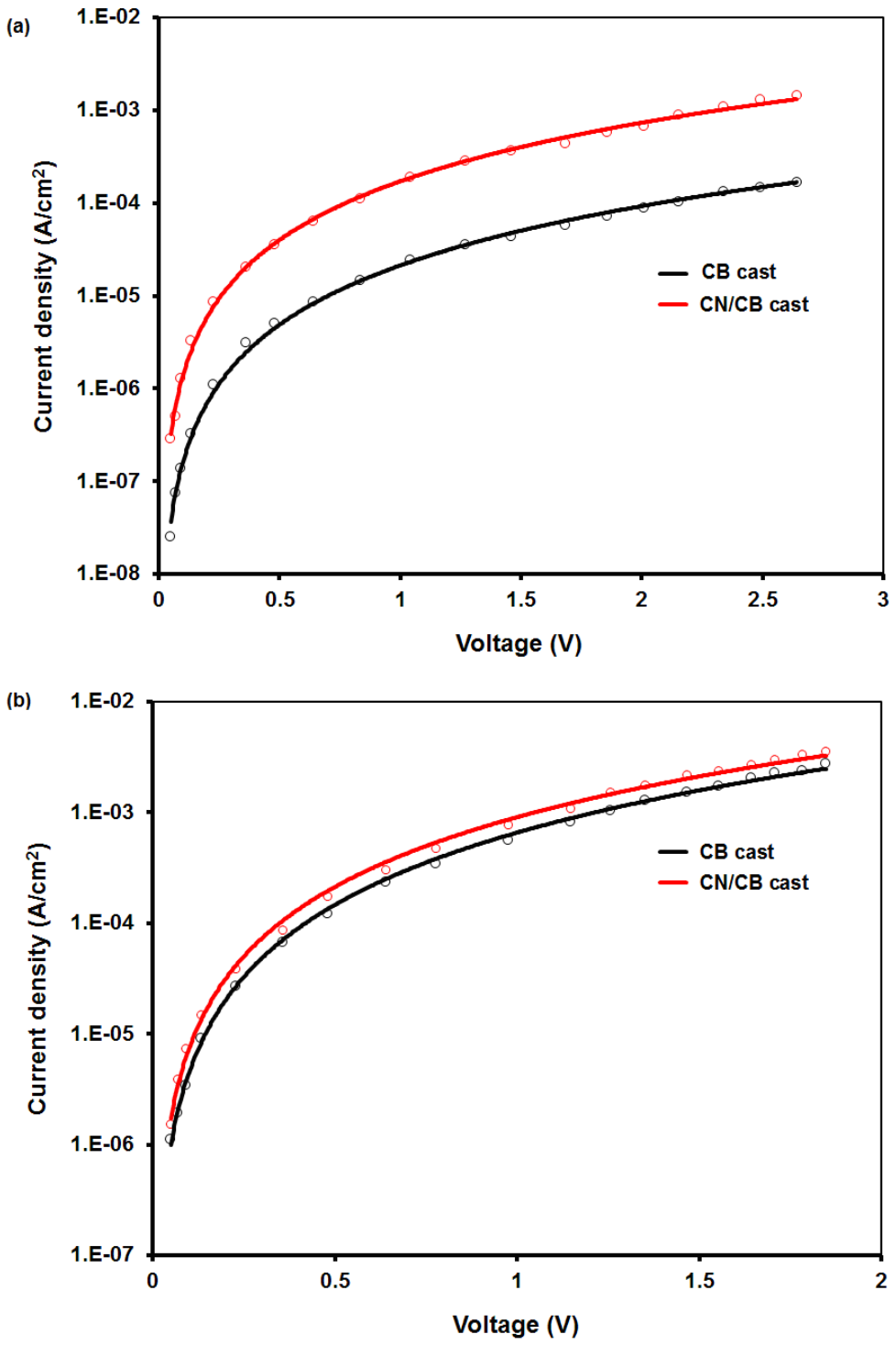

Figure 10. Current –voltage characteristics of the (a) hole only devices and (b) electron only devices based on **2**:$PC_{71}BM$ blends cast from CB and CN/CB solvents. Solid lines are SCLC fitted.